

Original papers

Developing an orientation and cutting point determination algorithm for a trout fish processing system using machine vision

Hossein Azarmdel^a, Seyed Saeid Mohtasebi^{a,*}, Ali Jafari^a, Alfredo Rosado Muñoz^b^a Department of Agricultural Machinery Engineering, Faculty of Agricultural Engineering and Technology, University of Tehran, Karaj, Iran^b Department of Electronic Engineering, University of Valencia, Burjassot, Valencia, Spain

ARTICLE INFO

Keywords:

Image processing
Trout fish
Fin detection algorithm
Automatic fish dimension extraction

ABSTRACT

Fish processing in small and medium fish supplying centers requires an intelligent system to operate on different sizes. Therefore, an image processing algorithm was developed to extract the proper head and belly cutting points according to the trout dimensions. The algorithm detects the fish orientation and location of pectoral, anal, pelvic, and caudal fins. In this study, each of the trout images was divided into slices along its length in order to segment the fins and extract cutting points. The channel 'B' of RGB color space was considered in both initial segmentation and fin detection stages among the examined channels of RGB, HSV, and L*a*b* color spaces. The back-belly and head-tail sides were detected with an accuracy of 100% based on gray intensity values and head to tail ratio, respectively. Furthermore, performing an analysis of variance (ANOVA) resulted in an F-value of 64.82 among the fins. Conducting a t-test among the mean intensity values of the fins and non-fin regions of channel 'B' resulted in the highest distinction with t-values of 90.30, 78.07, 74.28, and 86.01 with $p < 0.01$ for the pectoral, pelvic, anal, and caudal fins paired with the corresponding non-fin region, respectively. The results showed that the selected 'B' channel is the adequate one for fin segmentation. The fin detection process showed an overall sensitivity, specificity, and accuracy of 86.05%, 99.97%, and 99.87%, respectively. By solving the line determination error in 8.24% and the extra object error in 4.12% of the samples, the overall fin identification accuracy was 100%. Finally, after extracting the fin regions, the start point of the pectoral fin and the end point of the anal fin will be applied in the trout processing system as the head and belly cutting points, respectively.

1. Introduction

Trout fish (*oncorhynchus mykiss*) is from the salmon species and categorized as one of the most popular types of fish in the world. The color of the fish varies from gray to olive green from its back towards the sides, and changes to silver as it converges to the belly. The size and shape of trout may differ depending on the growing conditions (wild or cultured, and undernourished or fully fed fish). Thus, processing the fish is a specific operation suited for each case. Typically, trout fish is supplied to the markets in non-processed form, in fillets (often without bones), or as smoked fish (FAO 2013). In the case of non-processed fresh fish, some prefer gutted fish, others opt for gutted and beheaded, or just in fillets. Therefore, the developed automatic system must provide different processing options according to customer demand. Due to different physiological characteristics (length or thickness), extracting the precise cutting points is not assured as the fish is processed based on its weight. If the head is cut from a fixed position, a large amount of

fillet might be lost since the same weights can correspond to different dimensions of the trout. Moreover, extracting inappropriate cutting points can damage the fillet or lead to an incomplete belly cleaning process.

Currently, fish are processed by different machines used for single specific stages of scaling, beheading, gutting, or filleting, one after another. Fish processing factories combine these individual machines to process the whole fish. Some examples of the functioning systems are proposed by Grosselfholz and Neumann (2008), Ketels (2008), Paulsohn et al. (2010), and Ryan (2015). In some of these systems, the process is performed on a fixed size or previously sorted fish. On the other hand, there are some expensive intelligent fish processing machines, which can process the fish in large volumes, only targeted for big industries and not affordable for small or medium fish supplying markets and companies. Therefore, a system that can simultaneously process the fish in both head and belly is more complicated compared to the single functioning systems. This fact is crucial when the device is supposed to

* Corresponding author.

E-mail address: mohtaseb@ut.ac.ir (S.S. Mohtasebi).

process the fish of different sizes. In order to develop such a precise system, machine vision must be applied as the main functional data extraction section.

A typical Machine Vision System (MVS) consists of an image acquisition system, image processing, and statistical analysis (Hong et al., 2014). To adapt a fish cleaning system to the individual characteristics of each sample, developing a particular cutting, cleaning, and gripping tools to hold and clean the fish of different sizes and weights is required. Therefore, such a multifunctioning system needs a robust image processing algorithm to determine the beheading position, belly cutting start point, and belly incision length. Extracting exact functioning locations requires an imaging system which is not adequately provided by the individual length and thickness detection sensors. After proper cutting point determination, the cutting tools are ordered from the control unit to process the fish and guarantee a complete and optimal cleaning.

Image processing is considered one of the main parts of machine vision (Krutz et al., 2000). There are many image processing based studies on fish processing and aquatic product management and sorting systems. Strachan (1993) measured the size of the fish using 512×512 pixel images from an 8-bit per pixel camera inside the imaging box positioned on the top of a conveyor belt. He used a transparent conveyor belt with underneath lighting to separate different fish units and offer better fish edge detection procedure. Zion et al. (1999) categorized three types of fish using machine vision and artificial neural networks. Other machine vision based studies including size extraction, fish sorting, and species detection were done by Booman et al. (1997); Storbeck and Daan (2001); Misimi et al. (2007); Paluchowski et al. (2016) and Guttormsen et al. (2016). Han and Shi (2007) performed another study on bone detection. Other studies on fish cutting and beheading machines were conducted by Wu and De Silva (1993); Jain et al. (2001) and Buckingham et al. (2001).

Misimi et al. (2008) applied computer vision to grade Atlantic salmon (*Salmo Salar*). They extracted the size features from binary images for quality assessment and grading. In another study, Hu et al. (2012) used color and texture features to classify fish species using machine vision. They sent the captured images of a smartphone to the processing system to analyze the color and texture of the sub-images. They proposed the best classification, based on the extracted feature of the HSV color space. Dowlati et al. (2013) used machine vision to predict gilthead sea bream fish freshness according to the color changes in the eye and gill. They used RGB and L*a*b* color spaces for eye segmentation and feature extraction. Costa et al. (2013) measured the size, direction, and heterogeneity of the fish based on the edge analysis using image processing technique. Their purpose was to develop some tools for online fish grading in different species according to their size, gender, and heterogeneity. Poonoy et al. (2014) classified boiled shrimp's shape in a red-green-blue format using the shape features as the Relative Internal Distance (RID). They used multilayer Artificial Neural Networks (ANN) to train and classify the shrimps and proposed a 15-node model for the best classification. Khashman (2012) presented an automatic portion identification system to detect six different chicken portions using image processing and neural networks. The rotational invariant system was able to identify the segments regardless of their orientation with an overall accuracy of 97.57%.

In recent works, Atienza-Vanacloig et al. (2016) used vision-based discrimination of tuna individuals in grow-out cages through a fish bending model. They applied a 2D model to fit on the fish body while swimming. In their system, the alignment, bending and orientation of the fish was detected in their flexion movement. Later, Misimi et al. (2017) proposed a robust classification approach to segment blood defects of the cod fillets by processing fillet images. They applied deep Convolutional Neural Networks (CNN) and Support Vector Machine (SVM) to segment blood defects and grade different fillets based on their quality. They obtained 100% and 99% of accuracy in blood clod detection using CNN and SVM, respectively. Teimouri et al. (2018)

segmented the chicken portions and sorted them using a robust vision-based intelligent modeling approach. They proposed a new on-line method based on combined machine vision and both linear and non-linear classifiers to automatically categorize the portions. They applied two different speeds of conveyor belt including 0.1 ms^{-1} and 0.2 ms^{-1} . The overall accuracy of their system in two different speeds resulted in 94% and 93% to classify five different groups, respectively. Hernández-Ontiveros et al. (2018) developed a fish counter system using an embedded system. They were able to automatically count the ornamental fish in two marine species in the range of 0.5 cm to 2.3 cm under controlled lighting. The counting process was done by digital image processing with an accuracy of 96.64%. In other research, Issac et al. (2017) applied computer vision to investigate the quality and freshness of fish according to their segmented gills. They used a digital camera to assess the fish post-harvest quality in different storage days. They segmented the fish gill region and used RGB image data for quality prediction. Later, Muñoz-Benavent et al. (2018) proposed an enhanced fish bending model applied to the automatic tuna sizing system. They used computer vision to define a geometrical model for tuna discrimination using 2D images.

In order to find the ideal head cutting point and determine the length of the belly incision, machine vision provides useful data including the length, width, and fin positions. The head and belly cleaning subsystems will process the head and belly on the ideal extracted cutting points and length. Therefore, the processing steps can be adapted to the individual characteristics of each sample. This system will increase fish processing quality and decrease the number of manual tasks.

The complete procedure of orientation, safety, and cutting point determination algorithm of the trout processing system is explained in material and methods (Section 2). In this part, we describe our proposed approach in more details on how to detect the head-tail and back-belly sides, determine a centerline for fin identification, and eliminate any possible errors. In Section 3, we present the results and discuss the applied method to identify precise cutting points after the desired orientation of the fish is secured. The conclusions and future work are described in Section 4.

2. Material and methods

2.1. Fish samples and imaging system

In total, 97 trout samples ranging from 262 g to 622 g with an average of 421.88 ± 78.04 g and a total weight of 36.5 kg were selected in this study. Their length varied from 275 mm to 395 mm with an average of 324.8 ± 24 mm. The width also ranged from 60 mm to 90 mm with an average of 78 ± 5.8 mm. The samples were randomly selected from those fresh samples delivered to the self-service restaurant at the University of Tehran. A digital camera (Samsung EC-SH100 Wi-Fi Digital Camera with 14 MP, 5 × Optical Zoom) was used to capture the images. The imaging system consisted of a stainless steel case with six rows of the lights. Each row contains 72 light-Emitting Diodes (LED) installed inside the case. The images were captured under controlled condition. Both sides of the chamber were considered as low as possible to reduce the effect of ambient light. Based on the required power, an AC to DC power supply (S-180-12, input 220 V-output 12 V, 15 A) was applied to illuminate the case. The image acquisition setup is presented in Fig. 1. The image processing algorithm was developed using MATLAB 2013a software running in a Hewlett-Packard S4530 laptop computer with an Intel(R) i5-2410M CPU@2.3 GHz with 8 GB RAM. In order to conduct further assessment and observe the position of trout head, evacuated belly, and its spinal cord, an X-ray image was also provided by an X-ray setup (X-ray SEDECAL, APR-VET -Tube Support S2).

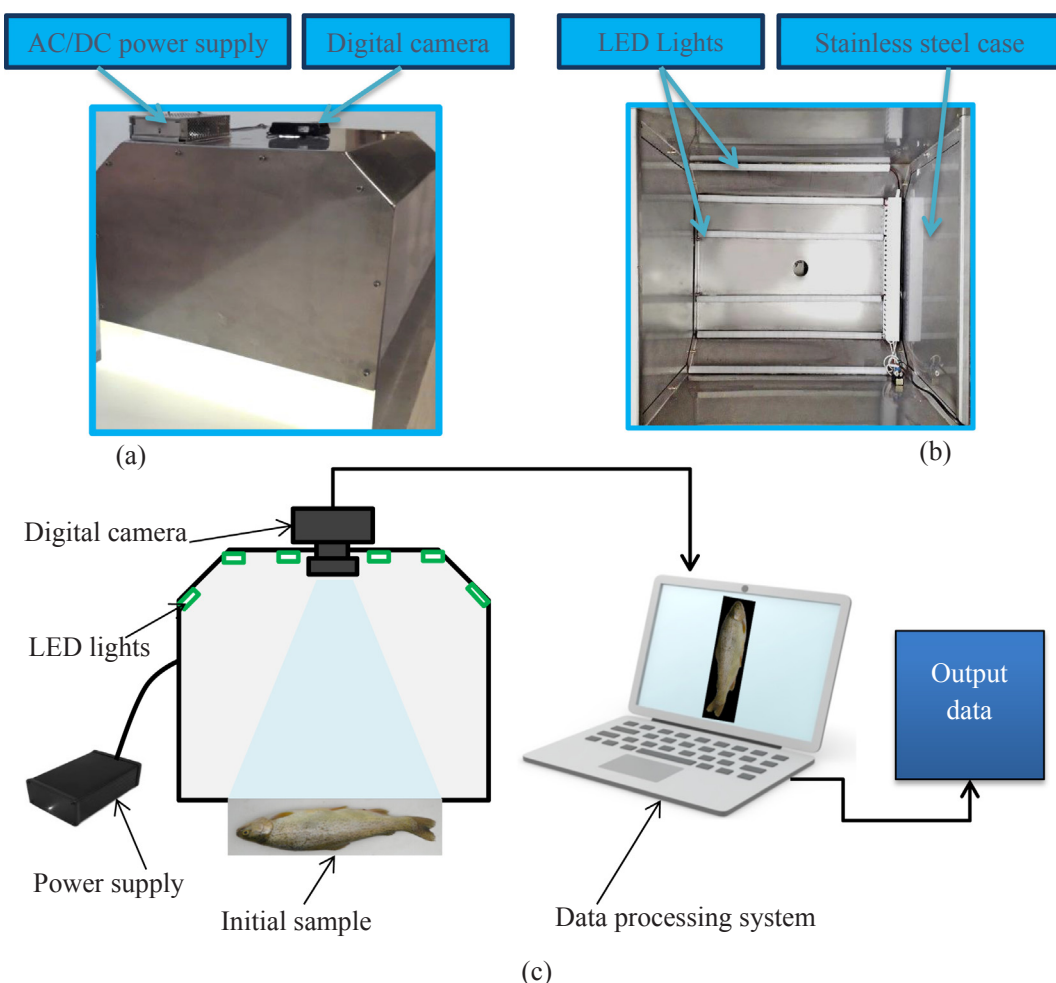


Fig. 1. Image acquisition setup: (a) imaging case, digital camera, and AC/DC power supply, (b) inside of the imaging case with six rows of LED lights installed in the stainless steel case, and (c) data acquisition setup.

2.2. Image processing and extracting trout characteristics

The entire image processing procedure is illustrated in Fig. 2. This figure shows the imaging case and trout moving direction. Some inappropriate positions of the trout together with the proper feeding position are presented in this figure. The appropriate feeding position is the belly towards the case with the head to the left side, which is shown with a check mark in Fig. 2. Any condition rather than this position will result in improper functioning of the system. Therefore, before performing any action by the machine, the image processing system detects whether the operator has considered the predefined feeding position or not. If the condition is approved, the functioning data will be sent to the control unit to process the fish; otherwise, the system will alert or stop.

The first step is preprocessing the image, including resizing, cropping, applying a manual threshold, filling the holes and removing any small objects rather than the fish. Later, the initial orientation of the trout is detected, and the real dimensions (length and width) are extracted. Then, the initial centerline is determined to detect the back and belly sides. Next, another line is defined to separate the belly side into two other parts to facilitate fin segmentation. Fig. 2 also shows two types of possible errors occurred during fin detection stage. Finally, the extracted positions of the fins will be applied in the functioning of the system. The detailed procedure is described in the following sections.

2.2.1. Trout segmentation from the background

Image segmentation is one of the significant steps of image

processing which directly influences the performance of other post-segmentation processes (Teimouri et al., 2014). In order to meet the food processing sanitary safety regulations, the conveyor belt must be considered from white food-grade materials. This fact imposes a specific image processing procedure; otherwise, the fish will be inappropriately segmented from the white background.

In general, a fast and automatic thresholding method is desired (Lin, 2005). So, like most of the typical image processing studies, we applied Otsu (1979) thresholding algorithm at first step. Since in some cases, the area near the trout chest and belly had similar pixel intensity values to those of the white background, the trout region was not completely segmented using this method. In order to improve the method, we noticed that the region of interest depends on the contrast between the fish sample and the background (Mendoza et al., 2006), then, all channels of 'RGB', 'HSV', and 'L*a*b*' color spaces were tested on the image (Fig. 3). Finally, the channel 'B' of the 'RGB' color space showed a high contrast between the pixel intensity values of the trout and the background providing the best results. Finally, a threshold intensity value of 150 was selected as the initial step in the segmentation process.

The initial image was captured in the dimension of 3240×4320 in rows and columns, respectively. This image was converted to a 736×351 matrix after resizing and cropping, considering a trade-off between the image quality and processing time. As the dimension of the initial image matrix is large, we resized the images to an optimized size regarding the balance between acceptable reduced image quality (preserve any required small objects like pelvic fins and their color features) and the computation time which gets more significant in fast

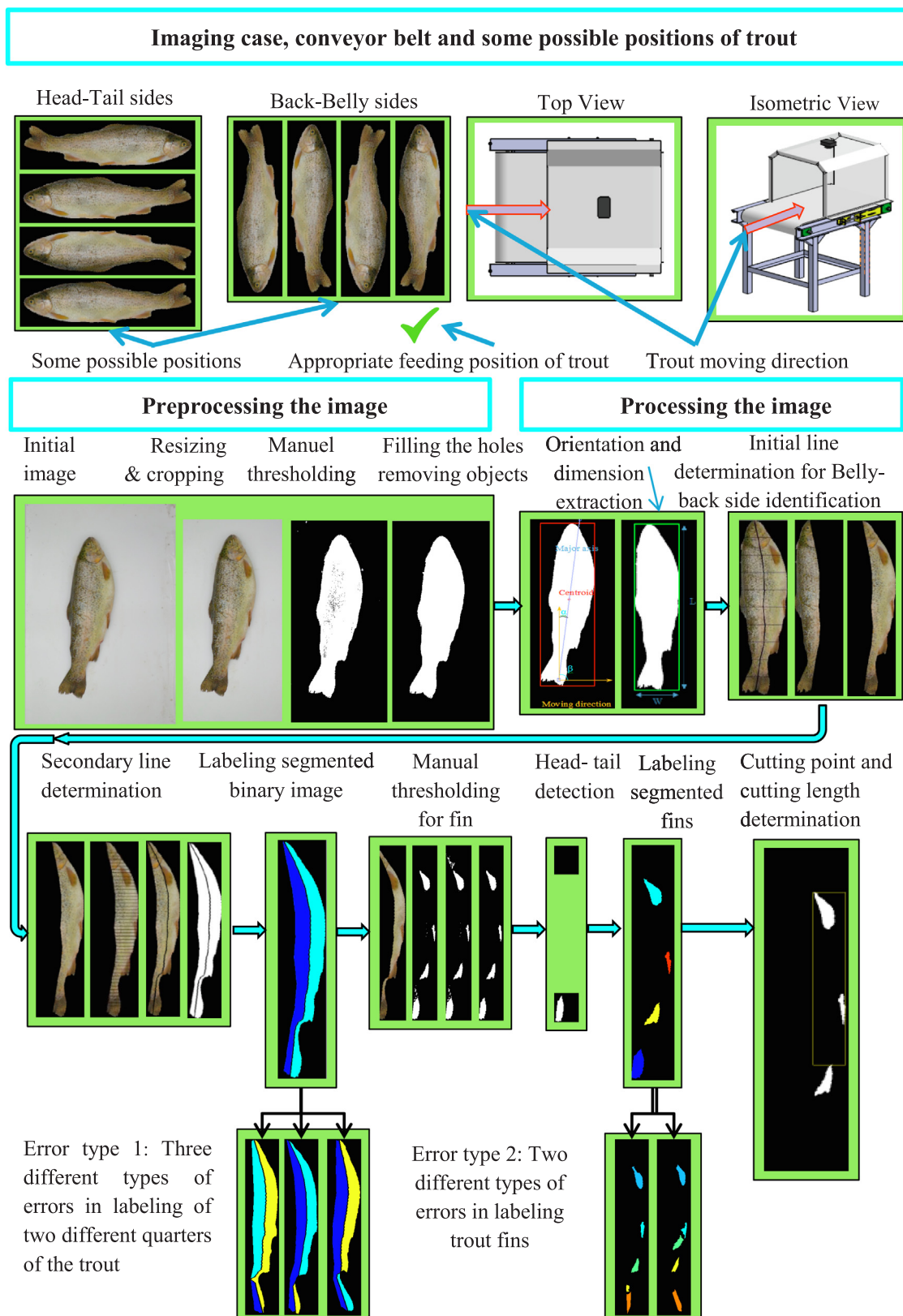


Fig. 2. The image processing procedure of the orientation and cutting point determination algorithm applied in the automatic trout processing system.

real-time systems. In the next step, the resized images were converted into the binary images (black and white): the pixels with intensity values lower than 150 were considered as '1' (white) and the rest were considered as '0' (black). Afterwards, some smaller areas apart from the

target (trout sample) still appeared in the background. On the other hand, some pixels inside the trout region were omitted (Fig. 4a). Thus, a 4x4 structure element was defined to remove the isolated pixels in the binary image and on the other hand, any possible holes in the trout

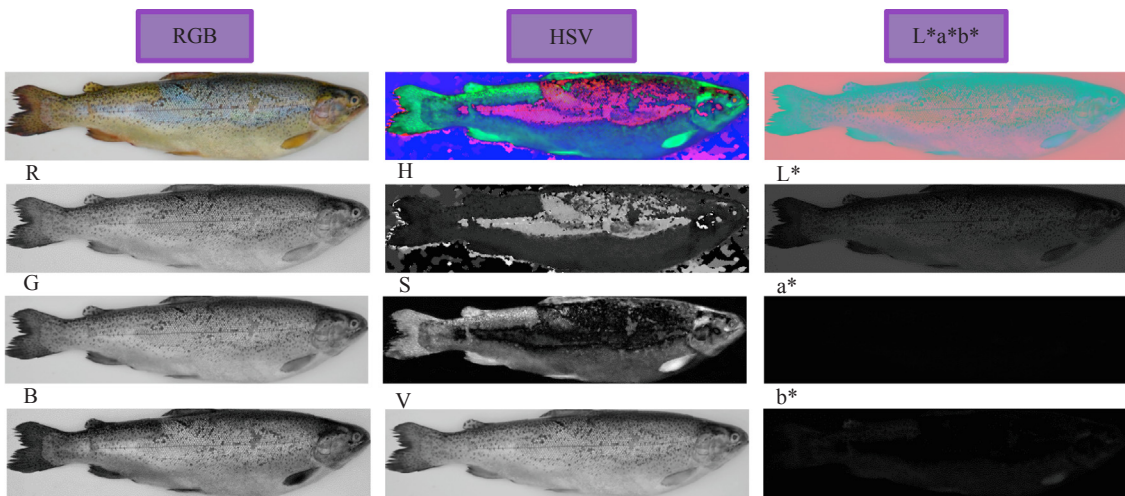


Fig. 3. RGB, HSV, and L*a*b* color spaces with related color channels examined in trout segmentation.

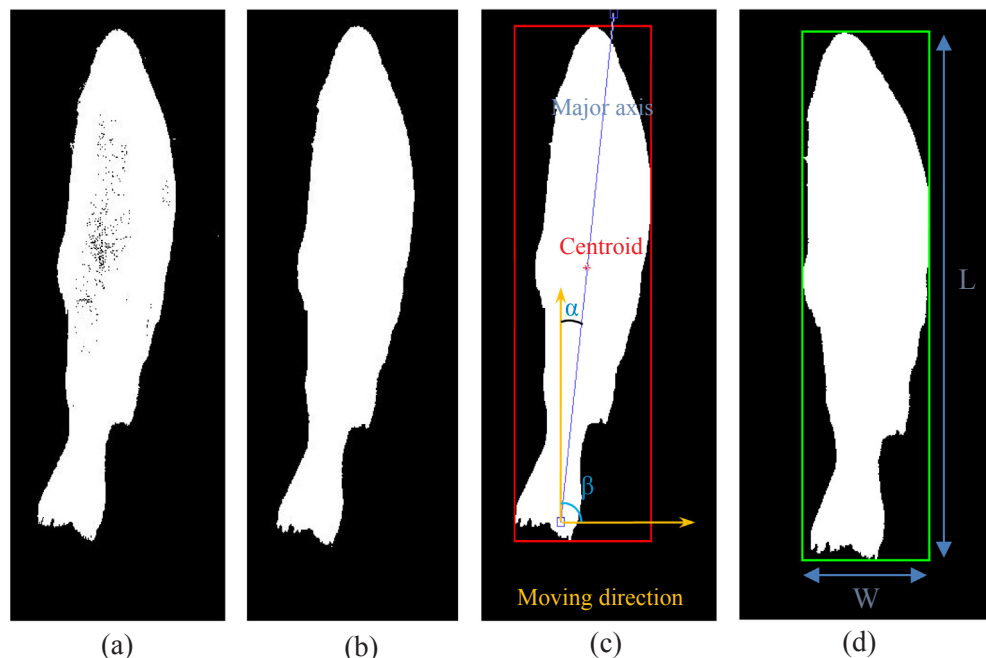


Fig. 4. Trout segmentation, bounding box correction and dimension extraction: (a) binary image of fish generated by applied threshold, (b) optimized image by removing any extra objects and filling the holes in the fish target, (c) fish centroid, major axis, differential angle ‘ α ’ and complementary angle ‘ β ’, and (d) the oriented fish image and corrected bounding box.

region were filled (Fig. 4b). Finally, the samples were completely segmented from the background. In this study, two different segmentation stages (sample-background and fish-fin) were performed.

It is common that fish samples are arranged in different positions, i.e., not aligned with the perpendicular moving direction of the belt. Before extracting the fish dimensions, each image is turned, so the results of all samples are comparable. In order to extract the real trout dimension, the following steps are done:

- (1) Defining the initial bounding box around the segmented fish (Fig. 4c).
- (2) Determining the major axis of the trout equal to the length of the major axis of an ellipse (in pixels) based on the normalized second central moment of the trout region.
- (3) Defining the complementary angle (β) between the major axis and moving direction.
- (4) Calculating the differential angle (α) and rotating the image as equal as ‘ α ’ to generate the new bounding box (De et al., 2013) to extract the exact length (L) and width (W) of the trout (Fig. 4d).

The extracted dimensions (length and width) are applied in the image processing algorithm as stated in the following:

- (1) The image was cropped in two different steps to reduce the computational load. In the first step, the initial image was resized, and a wide margin of the image was cropped to remove a significant part of the background (Fig. 2-resizing and cropping). In the next step, the image was cropped based on the second bonding box area (Fig. 4d) with the length of ‘L’ and the width of ‘W’. A sample of cropped image is shown in (Fig. 5a).
- (2) Defining two lines from 10% of the length in both sides and further seven lines between these two lines (Section 2.2.2).
- (3) Defining two lines from $\frac{1}{15}$ of the length of the fish from both sides along its length and further 45 lines between these lines (Section 2.2.3).
- (4) Defining structure element equal to 0.1% of trout bounding box area (described in Section 2.2.4).
- (5) Separating two areas (A1 and A2) to determine the head and tail sides by comparing the number of white pixels (described in Section 2.2.5).

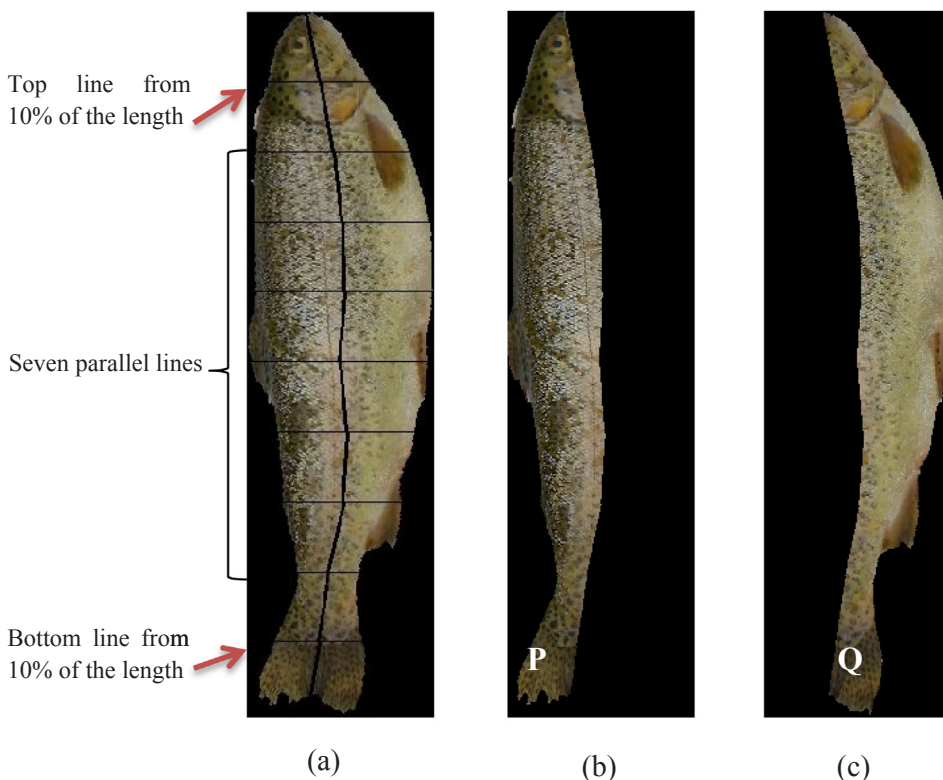


Fig. 5. Centerline determination for back-belly detection: (a) two lines from 10% of the width with seven parallel horizontal lines defines the center line by connecting the midpoints, (b) extracted image for back-side ‘P’, and (c) the extracted image for the belly-side ‘Q’.

After trout segmentation, defining the proper bounding box, and extracting the length and width, trout back and belly sides are determined in the following.

2.2.2. Initial line determination (initial division) for belly-back side detection

After fish position detection as shown in Fig. 2, two horizontal lines passing from 10% of the total length from the top and the bottom of the segmented trout were determined (Zion et al., 1999). Additionally, seven horizontal parallel lines were drawn between them, and their midpoints were connected to extract the central line. The horizontal lines and the obtained central line are shown in Fig. 5a. By determining the central line, the images are divided into two parts (P and Q) as shown in Fig. 5b and c. These parts were analyzed to identify the belly and back sides by comparing the gray intensity values of both parts (Strachan (1993); White et al., 2006). Since the color near the trout belly is lighter than its back, the part with greater mean gray intensity value is considered the belly side. The final result of the back-belly side determination is shown in Fig. 11.

2.2.3. Secondary line determination algorithm (secondary division) for the head-tail and fin detection

The two-dimensional (2D) intensity histogram of trout image in channel ‘B’ is represented in Fig. 6. The values of the fin pixels were less than 90 in most of the samples (dark blue pixels). As shown in this figure, the pixel values in back-left (BC-L) and back-right (BC-R) have similar intensity values as trout fins, which makes the fin segmentation process more difficult.

In order to have successful fin segmentation, part Q shown in Fig. 5c was divided into two other parts (Q-1 and Q-2) with a secondary centerline (Fig. 7b). This is done by determining the horizontal lines and connecting their center points (Fig. 7a) similar to the initial line determination process. Since part ‘Q-2’ is now a narrow area, it is necessary to define more horizontal lines compared to the initial line

(Fig. 5a). On the other hand, increasing the number of lines leads to an inappropriate centerline, which is not the desired one (Fig. 12). By examining a different number of the lines, a range of lines between 35 and 55 resulted in the most appropriate centerline in all the images. Finally, 45 horizontal lines were selected and drawn between two other lines, which were considered from $\frac{1}{15}$ of the trout length from the top and the bottom. These lines are shown in red color in Fig. 7a.

2.2.4. Fin segmentation

The object labeling process in Matlab software starts from the top left to the bottom right in the image matrix. Therefore, the region ‘Q-1’ on the left side of the center line will be labeled as ‘1’ and the region ‘Q-2’ on the right side will be labeled as ‘2’ (Fig. 7c). Afterwards, ‘Q-1’ was discarded since the fins are always located in ‘Q-2’. Back and belly identification step (Fig. 5) guarantees that the fins are in ‘Q-2’ even if the head of the trout is downward.

The next step is to segment pectoral (F1), pelvic (F2), anal (F3), and caudal (F4) fins. The position of F1, F2, and F3 will be used in the trout cutting process. The caudal fin is used to identify the head and tail sides. Alike initial trout segmentation step, channels of ‘RGB’, ‘HSV’ and ‘L*a*b*’ color spaces were tested for fin segmentation. Among them, channel ‘B’ was again considered the best one since it showed a better distinction between the fins and non-fin regions. The fins and non-fin regions are shown in Fig. 8a for all tested channels. In this case, the pixels with intensity values less than 65 were considered the fins and the rest were considered the background (non-fin region).

In the segmentation process, some small objects and spots appeared in the binary image (Fig. 7e). As these objects were redundant, they were removed by considering an appropriate number of pixels in the binary matrix. To avoid removing the fins, especially the smallest fin (F2), the objects (in pixel) smaller than 0.1% of the bounding box area ($W \times L$) were omitted since the fin area is in relation with the trout dimension. To fill any holes inside the fins, a morphological function of MATLAB software was applied in which the connected pixels of

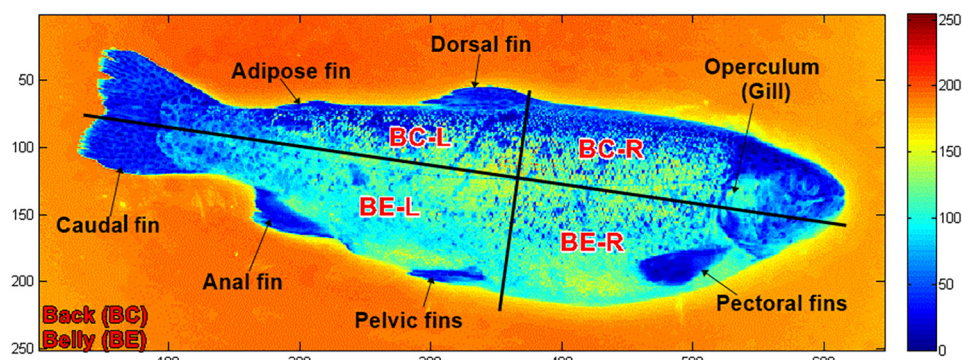


Fig. 6. The (2D) intensity histogram of trout in the range of [0–255]. This figure shows the difference between the trout and background. It also illustrates the difference between the intensity values of trout and its fins. (BC-L: back left; BC-R: back right; BE-L: belly left and BE-R: belly right).

background (logical ‘0’) change to foreground pixels (logical ‘1’) stopping the process as it approaches the object boundaries. Using the filling algorithm of morphological operations (Soille, 2013), the filled binary image can be written as Eq. (1):

$$J = \text{imfill}\{I, \text{'holes'}\} \quad (1)$$

where ‘I’ is the binary image matrix, ‘J’ is the binary image in which the ‘holes’ are filled. In morphological operations, a hole is defined as a set of background pixels that cannot be reached by filling in the background from the edge of the image (Wang, 2014).

The initial segmentation (segmenting the trout from the background) and secondary segmentation (fin segmentation from the region Q-2) were done based on manual thresholding. The initially applied method resulted in acceptable trout segmentation but, since the whole function of the system is based on the data received from the image analyzing section, it is essential to find the precise cutting points and

exact belly cutting length. Any inaccurate or incomplete fin segmentation will lead to improper functioning of the gutting and beheading subsystems. Therefore, the fin segmentation process is as critical as preprocessing and line determination steps.

Two further analyses were conducted to testify the channel ‘B’ performance in fin segmentation: *t*-test and analysis of variance (ANOVA). The *t*-test is applied to compare the most significant difference between two groups of data. In this case, it is desired that the difference between the mean intensity values of the fins and the corresponding non-fin area (Fig. 8b) results in higher *t*-values. This shows that there is a significant difference between the fin and non-fin region which facilitates fin segmentation. The analysis of variance (ANOVA) is applied among the mean intensity values of the segmented fins (Fig. 8c) in all the samples. In this method, the least ‘F’ value shows the least difference between the mean intensity values of the fins. The results of the *t*-test and ANOVA analysis are presented in Section 3.

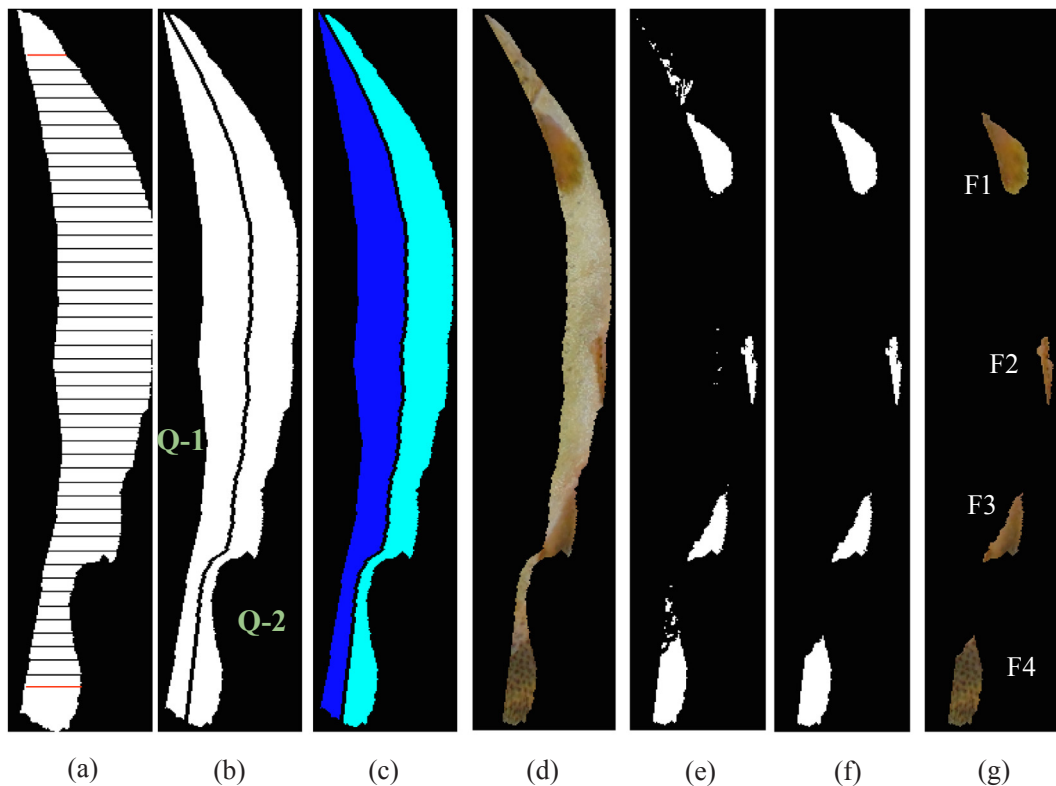


Fig. 7. Trout fin segmentation process: (a) defining 45 horizontal lines between two red lines from $\frac{1}{15}$ of the length from the top and the bottom of trout, (b) drawing center line in the binary image, (c) labeling the left side as ‘1’ (dark blue) and the right side as ‘2’ (light blue), (d) applying a mask to get the color image in part ‘Q-2’, (e) applying fin segmentation threshold, (f) removing extra object and filling any possible holes, and (g) final segmented fins (F1, F2, F3 and F4).

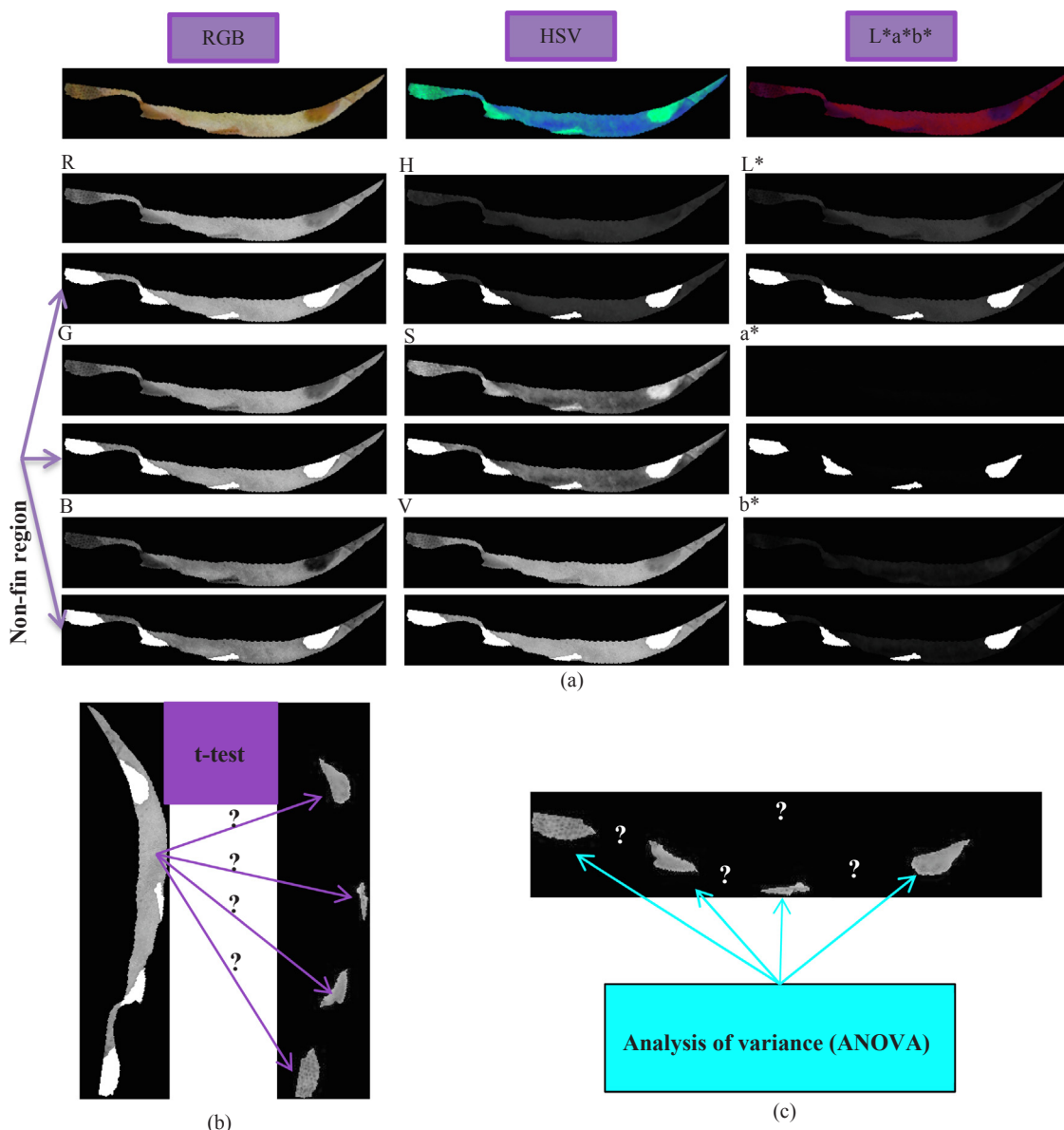


Fig. 8. Region 'Q-2' in RGB, HSV, and L*a*b* color spaces investigated in fin segmentation process. This figure also shows the non-fin region in which the fins are omitted: (a) The non-fin region and the fins are considered background and target, respectively, (b) the elements applied in the t-test (non-fin region & fins), and (c) elements of ANOVA analysis (fins).

The final result of the proper fin segmentation is also presented in Section 3. Beside the fin segmentation process, the real area of the fins has the most critical role in cutting point extraction. As shown in Fig. 13, if the visually selected channel was not the proper one, we were not able to rely on the fin segmentation results, which leads to exact cutting point extraction.

The statistical mean intensity values of each object (the fins and corresponding non-fin region) in each color channel were calculated using the following equation:

$$\text{Mean}(\mu) = \frac{\sum_0^M \sum_0^N I(i,j)}{n} \quad (2)$$

where 'i' and 'j' are the indexes of the pixels in the rows and columns, respectively. 'μ' is the color channel of each color space, 'n' is the number of the pixels of each object and, 'I' is the image matrix with the number of the rows of 'M' and the columns of 'N'.

The standard deviation of the mean intensity values (calculated with Eq. (2)) was calculated using Eq. (3).

$$\text{StandardDeviation}(\sigma) = \sqrt{\frac{(\mu_s - \bar{\mu}_s)^2}{s}} \quad (3)$$

where 'μ_s' is the object mean intensity value and 'μ̄_s' is the mean value of μ_s. In this formula, 's' is the number of the samples.

In order to determine the capability of the image processing algorithm for fin determination, 97 fish images (a total of 388 fins) were selected. The position of each fin was manually annotated and compared with the region obtained by the algorithm. Three common statistical parameters including Sensitivity (SE) (probability of a positive test result among those having the target category), Specificity (SP) (probability of a negative test result among those without the target category), and Accuracy (AC) (probability of both positive and negative test results among the target and non-target categories) describe the algorithm performance (Van Stralen et al., 2009), according to Eqs. (4), (5), and (6), respectively (Mjahad et al., 2017). This method is presented in Fig. 13 for a sample pectoral fin. In the following equations, the terms True Positive (TP), False Negative (FN), True Negative (TN),

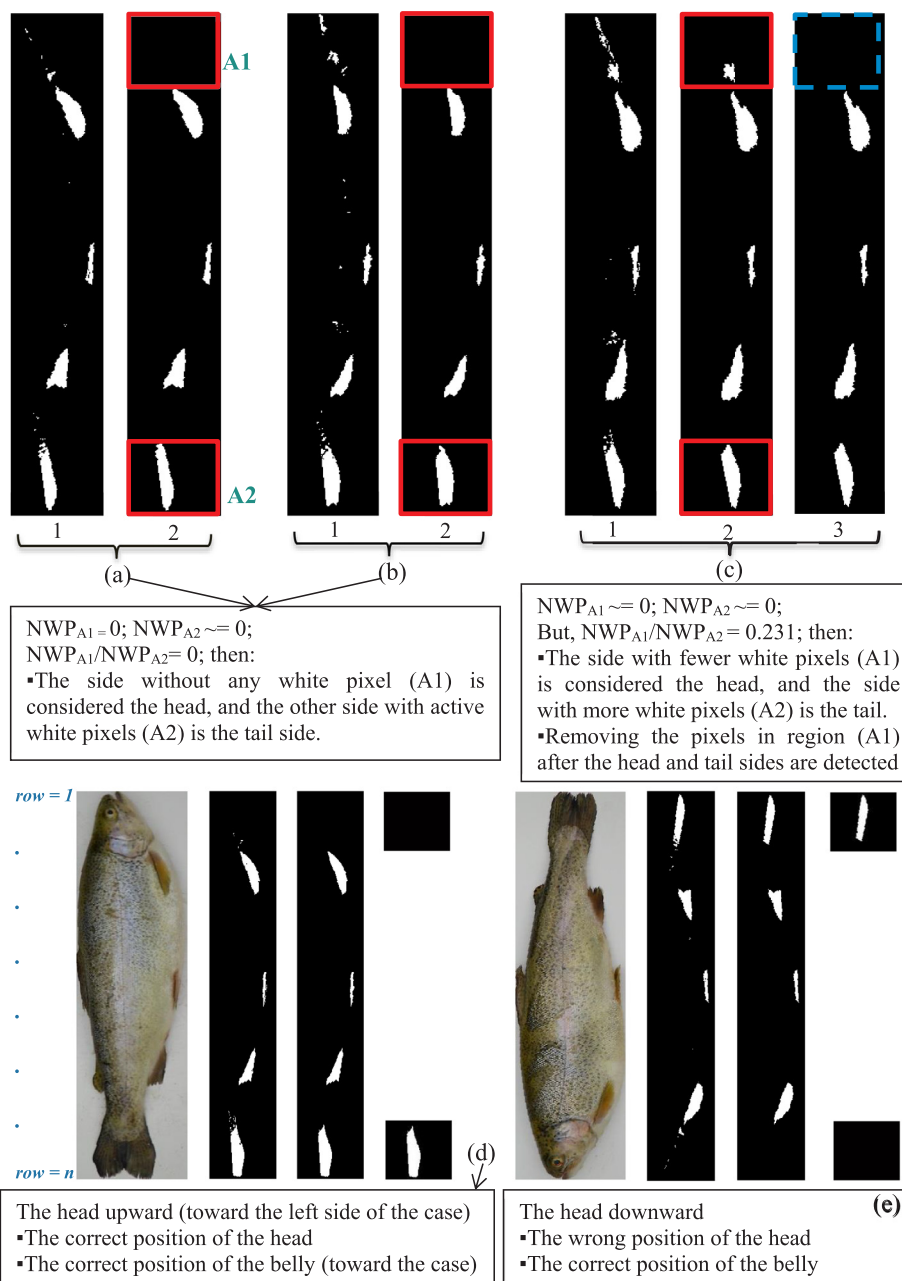


Fig. 9. Head and tail sides detection by comparing the number of white pixels in regions A1 and A2: cases (a) and (b) show that there are not any white pixels in region A1 while case (c) shows some white pixels in this region. In such cases, the white object in A1 was omitted after the head and tail sides were detected according to the applied criterion ($NWP_{A1} < NWP_{A2}$), (d) shows the desired position, and (e) is the wrong head-tail position. Both cases are tested as soon as the belly side is identified. (NWP: Number of the White Pixels).

and False Positive (FP) indicate the number of the pixels which are ‘correctly identified as fin pixels’, ‘incorrectly identified as non-fin pixels’, ‘correctly identified as non-fin pixels’, and ‘incorrectly identified as fin pixels’, respectively. The related results are presented in Section 3.3.

$$\text{Sensitivity} = \frac{\text{TP}}{(\text{TP} + \text{FN})} \quad (4)$$

$$\text{Specificity} = \frac{\text{TN}}{(\text{TN} + \text{FP})} \quad (5)$$

$$\text{Accuracy} = \frac{(\text{TP} + \text{TN})}{(\text{TP} + \text{TN} + \text{FN} + \text{FP})} \quad (6)$$

2.2.5. Head-tail side identification

In order to detect the head and tail sides, two regions (A1 and A2) were considered for further comparison. Both areas had an equal width of the image shown in Fig. 7a, and their length was considered 14.5% of the trout length. To determine the head and tail sides, the Number of the White Pixels (NWP) in the regions A1 and A2 were compared after final segmentation. In most of the cases, there were not any white pixels in the region A1 (Fig. 9a and b), but in some cases, there were still a number of the white pixels even after removing the objects smaller than 0.1% of the bounding box area (Fig. 9c). In total, three types of conditions were observed in region A1:

- (1) There were not any white pixels in region A1 after fin segmentation.
- (2) There were white pixels in region A1, but the isolated objects with

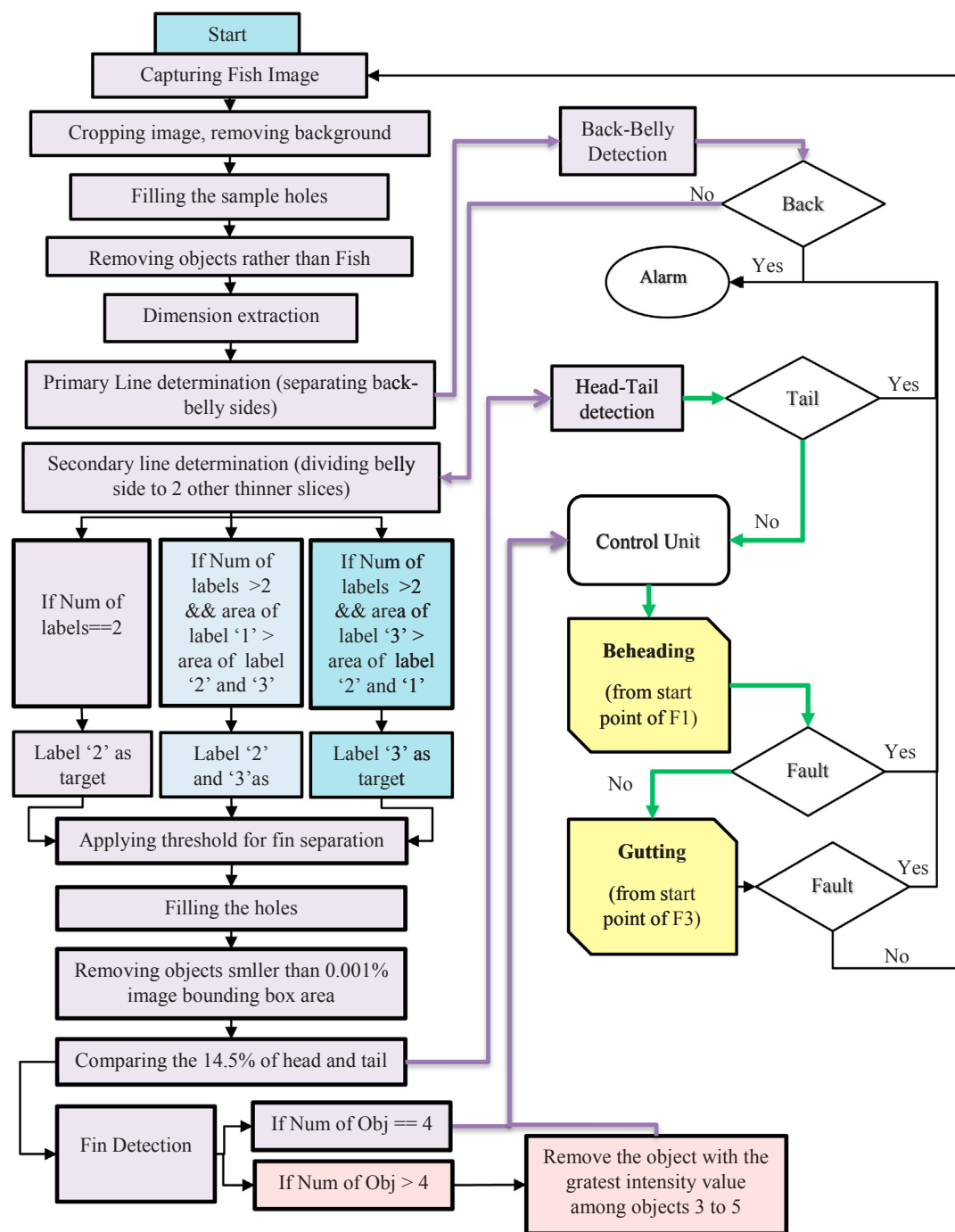


Fig. 10. Complete flowchart of the trout processing system including safety and alarming system, image processing, and beheading and gutting subsystems.

the number of the pixels less than ' ρ ' were removed (' ρ ' equals 0.1% of $W \times L$).

(3) There were still objects with more than ' ρ ' pixels in region A1.

For all samples, the number of pixels in A1 was less than A2, which resulted in $NWP_{A1}/NWP_{A2} < 1$. This criterion satisfied the head-tail side identification in all three conditions. Therefore, the sides with fewer and more pixels were considered as the head and the tail sides, respectively. The results are presented in Fig. 14.

The head of the trout must be in the left side of the imaging case with the belly toward the imaging case entrance. Therefore, as soon as the correct belly side is identified, the head-tail side will be detected. The possible head and tail sides of the trout are presented in Fig. 9d and e. The proper position of the trout in which the system can operate is

shown in Fig. 9d. By comparing the number of the pixels in both regions, if NWP_{A1} with corresponding low row value is less than NWP_{A2} , the fish head is upward (in the image) which is towards the left side of the imaging case. Both of these conditions (comparing the number of the active pixels of A1 and A2 and their row values) guarantee successful head-tail side identification.

2.2.6. Fin identification and cutting point determination

The complete flowchart of the image processing and safety systems together with the trout beheading and gutting processes is represented in Fig. 10. As it is shown in this figure, the malposition algorithm plays a critical role in system functioning. Any wrong fish position will lead to system failure or an improper process of the fish. Thus, before activating any function in gutting and beheading subsystems, the vision

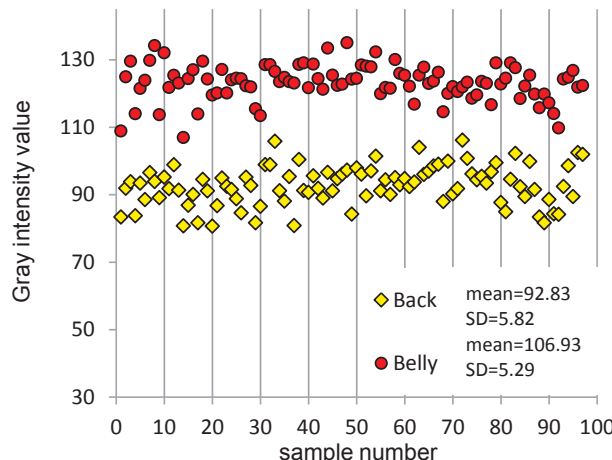


Fig. 11. The intensity values of the gray image for both back and belly sides of trout.

system checks the position of the samples according to the written image processing algorithm. In the case of improper position, the system will automatically alarm or stop the process. Finally, if the initial condition is fulfilled, the control unit will send the extracted data of the fins to the gutting and beheading subsystems.

Apart from the system safety, the functioning of the system depends on the proper fin segmentation and its position. In this case, the position of F1 is considered the head cutting point, and the position of F3 is the start point of belly incision towards its head. This incision length is enough to evacuate the belly content. The proper cutting region is depicted in Fig. 16. The complete procedure with the related results is discussed in Section 3.5.

Thus, in order to reach a successful fish cleaning procedure, three principal steps must be provided:

(a) Safety system functioning:

The proper fish positions are checked according to the following steps:

- (1) The image processing algorithm checks whether the trout belly is toward the imaging case (Fig. 2 and Fig. 5). This is done by comparing the gray intensity values of both back and belly sides.
- (2) The final safety test is performed to determine the head and tail sides after the belly side is correctly identified. In this case, there are just two conditions: belly toward the imaging case with the head upward or downward. The desired position is presented in Fig. 9d. In this figure, the head is supposed to be positioned upward (toward the left side of the imaging case).
- (a) Extracting the proper cutting points.
- (b) Operation of the head and belly cutting subsystems based on extracted fin positions.

3. Results and discussion

The obtained results are described in detail according to the developed image processing algorithm as following:

3.1. Back-belly side identification using an initial line (initial division)

After the initial line was determined, trout back and belly sides were identified according to their gray intensity values. The result of the intensity values is shown in Fig. 11. The values for the back and belly sides are shown in yellow and red colors, respectively. As the back of the trout is darker than the belly side, the back side showed a mean

value of 92.83 with 5.82 of standard deviation while the mean value of the belly side was 106.93 with 5.29 of standard deviation which showed successful back-belly side identification in all of the tested samples.

3.2. Secondary line determination (dividing part Q into two parts of Q-1 and Q-2)

As stated in Section 2.2.4, considering two labels can satisfy fin segmentation process, but an improper central line will lead to the incorrect fin segmentation process. In other words, we must separate the belly side into two parts with labels '1' and '2' (Fig. 7c) in which the part with label '1' is omitted. Examples of incorrect labeling (three labels) and the wrong detected fins are shown in Fig. 12.

In secondary line determination step, three types of errors including error type '1' (E1), error type '2' (E2), and error type '3' (E3) were observed. 'E1' occurred when we considered more lines. In this case, as the number of horizontal lines increases, the center of a horizontal line comes close to the anal fin (case 'b' of E1) which guides the centerline to fall out of the fish area in distorted anal fins. On the other hand, considering a low number of horizontal lines results in an improper line which is not passing through the center, causing problems in the narrowest region of the fish ('E2').

The third type of error (E3) occurred when one horizontal line was not properly created. Even though an increased number of lines decreased the errors, in case of 45 lines, there were seven errors including four errors of both 'E1' and 'E2' and three errors of 'E3'. In order to solve these errors, two different comparative conditional statements were added to the algorithm. Determining the centerline is critical since the fin detection process depends on this step. As it is shown in Fig. 12, in cases of 'E1' and 'E2', the area (in pixels) of blue color with the label '1' is greater than the area of yellow and light blue colors with the corresponding labels '3' and '2'. In these cases, both labels '2' and '3' were considered the target for further fin detection process and the region with label '1' was discarded. In the case of 'E3', the area of label '3' with a corresponding yellow color is greater than the area of both labels '1' and '2'. In this case, the label '3' was considered the target. The conditional comparison procedure is depicted in the operational flowchart shown in Fig. 10. This procedure led to appropriate fin segmentation in all 97 trout samples.

3.3. Fin segmentation

Once the region 'Q-2' is properly defined, the fins are segmented using the selected 'B' channel. This channel was manually selected according to the trial and error based on the best visual segmentation but, as this step is crucial in cutting point determination; two further analyses were conducted to testify the channel 'B' performance among all other color channels including the following stages:

- (a) Determining the least difference among the fins: To testify the selected channel performance, we performed an analysis of variance (ANOVA). In this case, the F-value is considered a criterion to evaluate the color channel performance (the procedure is shown in Fig. 8c). In ANOVA analysis a greater F-value indicates a more statistically significant difference between the mean values of the groups (Lee et al., 2014).
- (b) Investigating the most significant difference between the mean intensity values of the fins with the corresponding non-fin region (the procedure shown in Fig. 8b): the more significantly different the mean intensity values are, the higher the t-value will be obtained.

Table 1 shows the results of the mean 'B' intensity values together with the other eight tested color channels of RGB, HSV and L*a*b*. In all the cases, the averages of the mean intensity values are significantly different among the fin groups ($\rho < 0.01$). As stated in the table, the

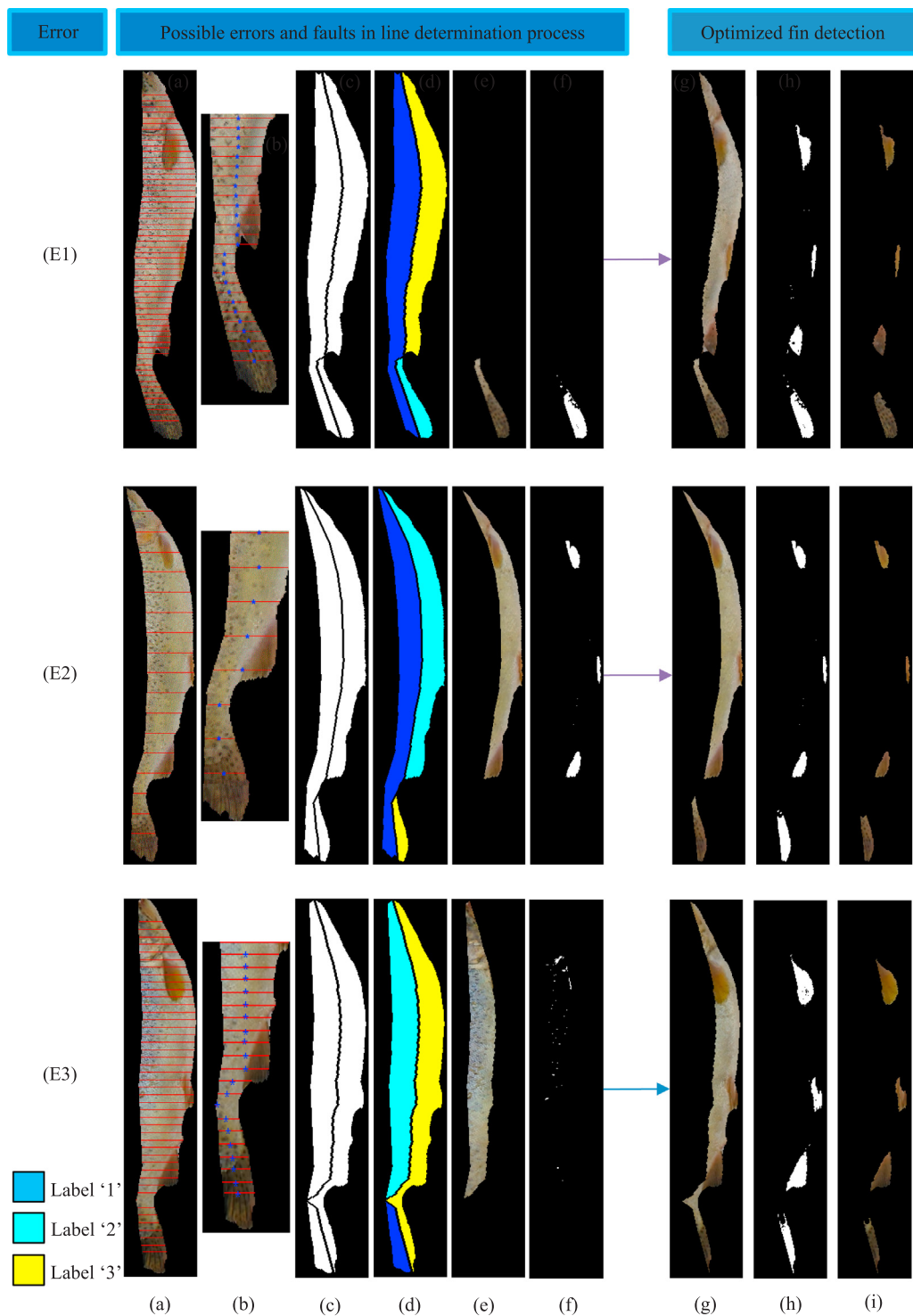


Fig. 12. Three different errors in secondary line determination step which leads to an incorrect segmentation: (E1) applying excessive number of horizontal lines causes incorrect labeling in distorted anal fins, (E2) considering a low number of horizontal lines, and (E3) indexing problem in the start and end point of the line in some samples.

average values of channel 'B' for F1, F2, F3, and F4 are 33.78, 43.73, 40.94, and 38.78, respectively. The results show that channel 'H' has the least F-value (32.00) among all tested groups. This means that the mean intensity values of the fins are close to each other, which is desired for fin segmentation. Among them, channel 'B' has a second place with the F-value of 64.82.

Although the F-value of channel 'H' is less than the value of channel 'B', Fig. 3 shows a higher visual distinction of channel 'B' compared to

channel 'H' between the fin and non-fin regions. This fact is proved by conducting a t-test between the fin and non-fin intensity values in all the color channels. The result of the t-test is presented in Table 2. As it is shown in this table, the t-values of channel 'B' for the paired groups of the non-fin region and each of the corresponding fins are 90.30, 78.07, 74.28, and 86.01 for F1-non-fin, F2- non-fin, F3-non-fin, and F4-non-fin, respectively. The mean value of t-test is 82.16 which is the highest value among the tested channels. Thus, these results prove that the

Table 1

Results of one-way analysis of variance (ANOVA) between the groups of the fins.

Color channels	(mean intensity value \pm SD)				F value
	F1	F2	F3	F4	
R	107.55 \pm 10.30	115.23 \pm 11.11	88.30 \pm 11.81	73.65 \pm 10.62	96.19 \pm 19.64
G	80.31 \pm 9.53	84.51 \pm 9.63	64.43 \pm 9.41	59.63 \pm 7.86	72.22 \pm 13.81
B	33.78 \pm 5.60	43.73 \pm 5.31	40.94 \pm 5.37	38.78 \pm 4.17	39.31 \pm 6.29
H	0.101 \pm 0.01	0.095 \pm 0.10	0.085 \pm 0.02	0.099 \pm 0.01	0.096 \pm 0.02
S	0.684 \pm 0.06	0.062 \pm 0.06	0.531 \pm 0.07	0.466 \pm 0.08	0.576 \pm 0.11
V	0.422 \pm 0.04	0.452 \pm 0.04	0.346 \pm 0.04	0.289 \pm 0.04	0.377 \pm 0.08
L*	22.68 \pm 2.41	24.15 \pm 2.46	18.59 \pm 2.55	16.75 \pm 2.18	20.54 \pm 3.83
a*	-0.921 \pm 0.69	-0.114 \pm 0.26	-0.055 \pm 0.07	0.258 \pm 0.27	-0.337 \pm 0.52
b*	20.11 \pm 3.93	18.26 \pm 3.45	11.08 \pm 2.95	9.19 \pm 2.56	14.66 \pm 5.66

The F-value indicated a significant difference between the mean values of the four tested fin groups at the 99% probability level ($p < 0.01$).**Table 2**

Results of t-test between the groups of the non-fin and the fins in corresponding color channel.

Color Channel	(Non-fin region mean intensity value \pm SD)	t-value				Mean of t-value
		F1	F2	F3	F4	
R	141.85 \pm 6.03	36.42	25.71	43.80	59.94	41.47
G	132.71 \pm 6.15	58.19	51.12	65.72	75.85	62.72
B	106.48 \pm 7.61	90.30	78.07	74.28	86.01	82.16
H	0.13 \pm 0.00	20.81	28.64	19.25	20.92	22.40
S	0.25 \pm 0.04	65.00	59.39	35.35	18.01	44.44
V	0.56 \pm 0.02	36.46	25.79	43.82	59.94	41.50
L*	36.39 \pm 1.65	66.14	49.94	63.24	73.82	63.29
a*	1.52 \pm 0.48	23.04	26.83	30.54	29.86	22.18
b*	0.84 \pm 0.36	48.43	49.35	35.03	35.03	41.96

The t-value indicated a significant difference between the mean values of the tested paired fin and non-fin groups at the 99% probability level ($p < 0.01$).**Table 3**

Image processing Sensitivity, Specificity and Accuracy values of four trout fins.

	Pectoral Fin (F1)	Pelvic Fin (F2)	Anal Fin (F3)	Caudal Fin (F4)	Overall
Sensitivity%	81.251	75.760	88.546	98.662	86.054
Specificity%	99.964	99.968	99.975	99.951	99.965
Accuracy%	99.774	99.893	99.892	99.938	99.874

visually selected 'B' channel is adequate for trout fin segmentation.

Concerning the fin detection results, Table 3 presents the percentage of fin detection values including sensitivity, specificity, and accuracy. The most and the least sensitivity values correspond to F4 and F2, respectively. The reason for the low sensitivity of F2 is its smaller size compared to the other three fins. Since F2 is under the belly, only a small amount of this fin is visible in this view. Fig. 13 shows a sample pectoral fin. The sensitivity value of F1 was lower than F3 and F4. This is due to the thin glassy area of the fin at the joint of the fin and the body which shows the color of the underneath skin. Since the area of F3 is greater than F1 and F2 and its intensity value is less than both fins, the sensitivity of this fin is more than the other two fins. Finally, the highest sensitivity value was calculated for F4 because of the high thickness and slight change in the pixel intensity.

Misimi et al. (2017) reported color based, pixel-wise and SVM-based model, developed for accurate segmentation and localization of blood defects in cod fillets with the overall accuracy of 96%. Our results showed an overall accuracy of 99.88% for the fin segmentation. It should be considered that the most significant criterion among these three criteria is the sensitivity since it considers the number of the target pixels (fins) rather than non-target pixels, which is greater than the target pixels in most of the cases. In this research, the overall sensitivity was 85.54% for all the fins.

3.4. Head-tail detection

As shown in Fig. 9, the head side (region A1) typically indicates few or no pixels, while the tail side (region A2) has active pixels in all the samples. In the fin segmentation step, as the threshold was considered to be 65 based on trial and error, we found that this criterion could satisfy successful fin detection in all the samples. The proof of this claim is presented in Table 3. Among the segmented fins, this method resulted in the highest sensitivity and accuracy values for the caudal fin. Therefore the existence of the pixels in region A2 (caudal fin) with the lack of pixels (no white pixels) in region A1 is an ideal condition in which A1 and A2 can be considered as head and tail sides respectively. Despite our interest, there were some white pixels in region A1 in some of the samples. Therefore, we considered a criterion that can satisfy the head and tail side detection in all the samples. As stated in Section 2.2.5, by comparing the white pixels in the binary image, the ratio of the number of the pixels in A1 to the number of the pixels in A2 was considered as the head-tail detection criteria. As shown in Fig. 14a, no white pixel appeared in A1 in most of the samples. In other samples, the number of the pixels in region A1 (yellow markers) is less than the number of the pixels in the corresponding sample in region A2 (red markers). In this figure, the values are sorted in ascending order according to the number of the pixels in region A1.

The results of the NWP_{A1} to NWP_{A2} ratio is presented in Fig. 14b. This ratio is categorized into six classes. According to this figure, in 43.30% of samples, the NWP_{A1} to NWP_{A2} ratio was equal to zero. Besides, 28.87% of fish samples fell into the second category with the ratios in the range [0.01–0.1]. The third category with the ratios in the range [0.11–0.3] contained 22.68% of the samples. These three categories altogether covered 94.87% of total samples with the ratios between [0–0.3]. Among them, just 3.09% and 2.06% of the samples fell into the fourth and fifth categories, respectively. No sample fell into the sixth category since in none of the samples the ratio was bigger than 0.75. Finally, as the calculation of the NWP_{A1}/NWP_{A2} resulted in less than '1' in all the samples, the regions with fewer and more pixels are considered the head and the tail sides of each trout, respectively. Therefore, this method guarantees the head-tail side detection in all the samples based on the compared number of the pixels of both sides with 100% accuracy. As the head and tail of trout are defined, all extra objects are removed in the head region (Fig. 9c) to avoid any possible problem in the fin detection process.

3.5. Fin identification and cutting point determination

Among all the images, there were four samples in which some extra objects were wrongly segmented in fin detection stage between F2 and F4. Examples of these images are shown in Fig. 15. These objects will cause system malfunctioning especially in belly cutting point determination, which is supposed to cut the belly from F3 towards the trout head. To remove the extra objects, a possible solution is to consider a

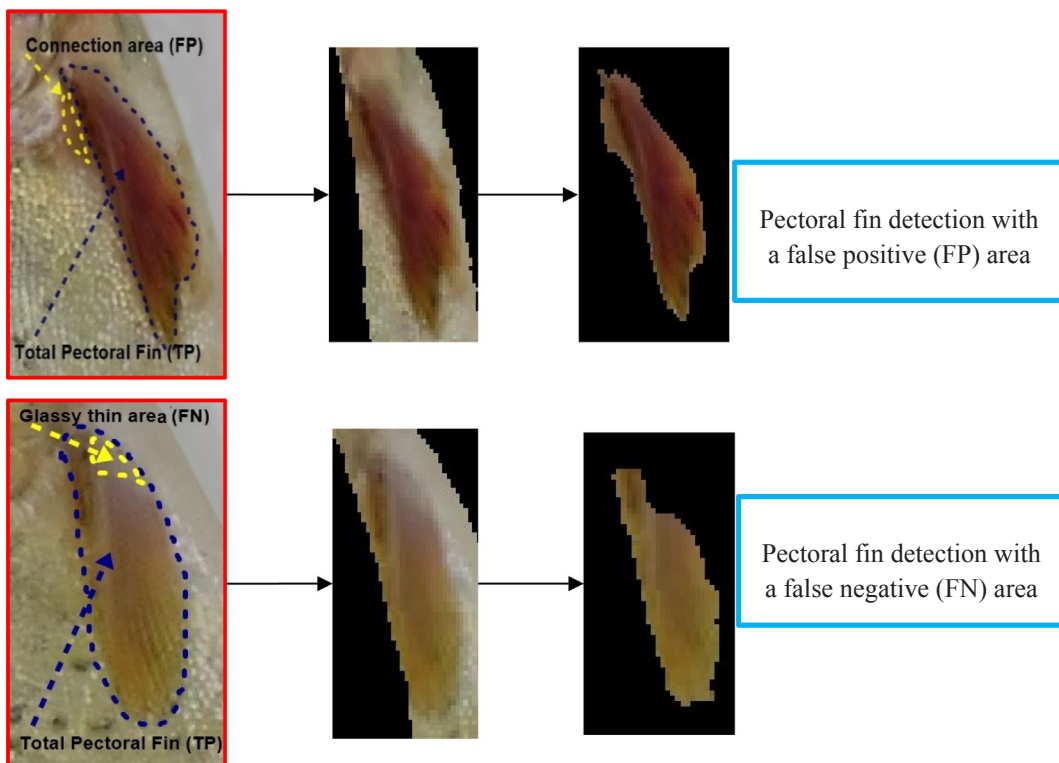


Fig. 13. Fin detection process in different possible conditions showing the fin segmentation sensitivity, specificity and accuracy calculations.

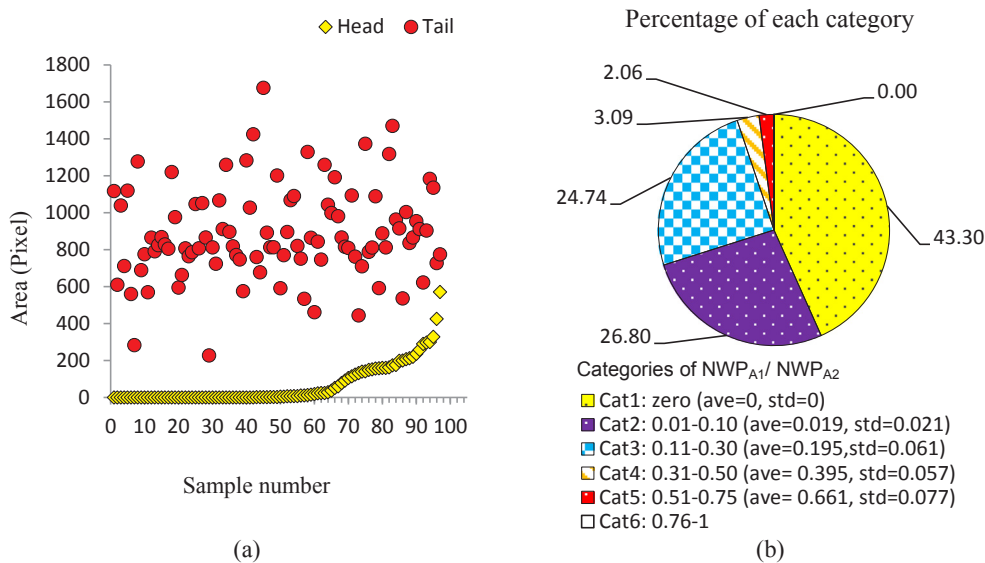


Fig. 14. (a) The number of the white pixels in region A1(head region) and A2 (tail region) sorted in ascending order according to the number of pixels in region A1, and (b) six defined categories of NWP_{A1}/NWP_{A2} and their related percentage in 97 samples.

greater structure element, but it results in omitting F3 in some samples because of its small area. Another solution is to eliminate the extra object with label '4' between F3 and F4, but among the mentioned images there were two images that the extra object was segmented between F2 and F3 (case 2). In such conditions, the anal fin (F3) was wrongly omitted. To avoid such problems, we considered the mean intensity values of channel 'B' as a criterion in which the object with the highest mean intensity values (the lighter object) was discarded.

Since the area between F1 and F2 is lighter with fewer dots and other dark spots, no further object was detected in this region. Thus, apart from the intensity value of F1, the intensity values of the other fins, together with the extra objects were considered for further

comparison. Among all 97 trout images, four samples were observed with an extra object. These objects had the mean 'B' intensity values of 56.92, 96.28, 55.41 and 53.00. These values were significantly different from 'B' intensity values of the fins presented in Table 1. Therefore, the extra object with the maximum mean 'B' intensity value was eliminated among the objects. Finally, in all the trout samples, the fins were successfully detected with 100% accuracy.

The detailed results of fin segmentation in all the samples, including three types of error in secondary line determination step (presented in Fig. 12) and two different cases of extra object segmentation (Fig. 15) are presented in Table 4. Among the samples, there was not any case with six detected objects, but even in such cases, as the mean intensity

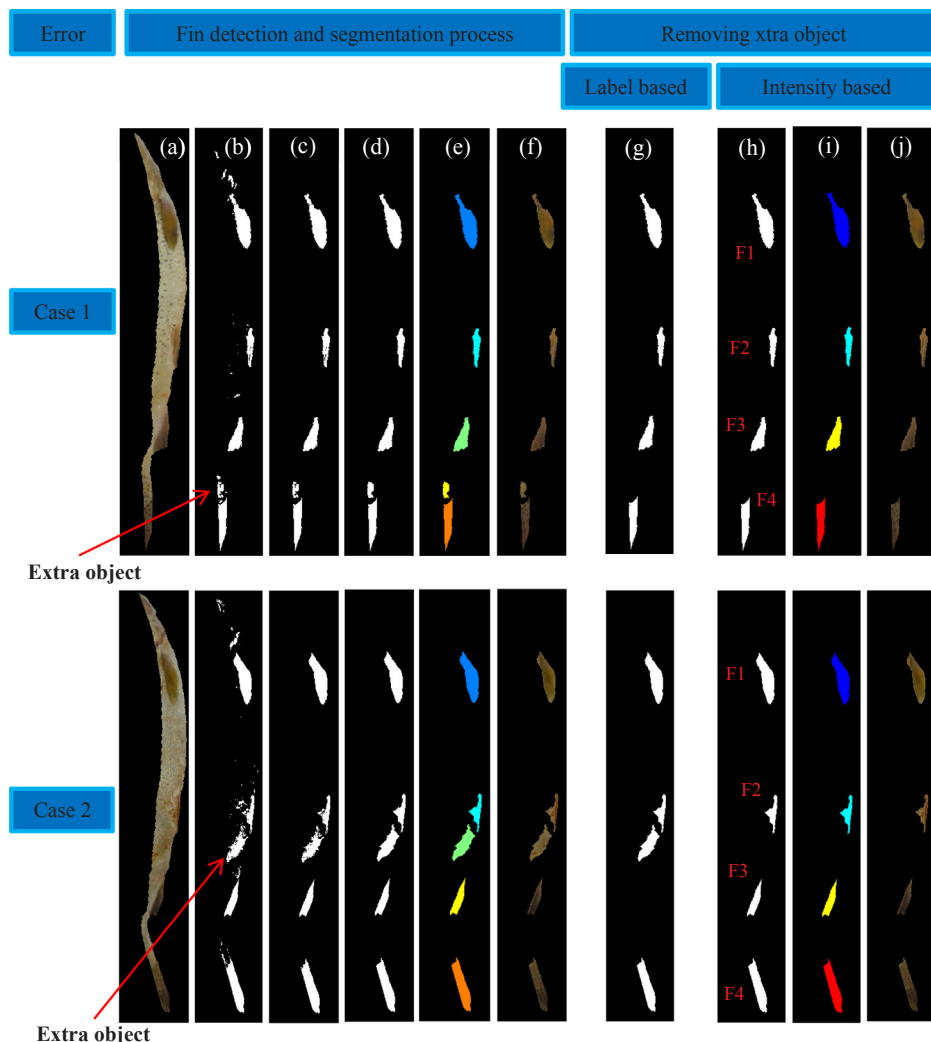


Fig. 15. Fin segmentation and extra object elimination in fin detection process in the region between F2 to F4: (a–f) fin segmentation procedure, (g) label based non-fin object removing, and (h–i) intensity based non-fin object removing.

Table 4

Detailed fin segmentation results with corresponding errors in line determination and fin identification steps with successful detection and final results.

Total errors of secondary line determination and fin identification (%)			SDWE (%)	FD (%)
12.37			87.63	100
Line determination error (%)		Fin identification error (%)		
8.24		4.12		
E1(%)	E2(%)	E3(%)	Case 1 (%)	Case 2 (%)
4.12	1.03	3.10	2.06	2.06

SDWE: Successful detection without errors; FD: Final detection.

values of the channel ‘B’ is determined for the fins and any possible extra object, the first two objects with the least intensity values will be considered F3 and F4.

As shown in this table, among all the samples, 8.24% of the images have the problem of line determination error. The percentage of the error types ‘E1’, ‘E2’ and ‘E3’ were 4.12%, 1.03%, and 3.10%, respectively. As stated above, in 4.12% of images, some extra objects were detected as trout fin. The extra object error was 2.06% for each of the cases. In total, 12.37% of the images had both line determination and extra object segmentation problem and the rest of the images were properly segmented. By removing both types of errors, the total fin detection value was 100% for all 97 trout images.

The desired function of the trout processing system is obtained when the head is properly cut with the least fillet lost. On the other hand, any extra object rather than the fillet, close to trout head, must be removed. Therefore, the cutting process will be performed from the beginning point of F1 in which the removal of the bony area near the fish gill is achieved (Fig. 16a).

In a trout processing machine, after beheading, the next step is to cut the belly and clean its internal content. In this design, the gutting process will be easily done since at the end of the fish path there is no obstacle for the evacuating tools. Fig. 16a shows the processed area of the belly in X-ray image with yellow dash lines together with beheading and gutting points. Since the belly intestines are located in the distance between the anal fin and the gill, F3 is chosen as the appropriate position to start the incision in the belly. Afterwards, a suction tube with a rotary cleaner brush will clean the abdominal cavity from the anal fin towards the head.

The position of F2 is determined to extract the belly arc together with identifying the processing rectangle (Fig. 16c). In this figure, the distance from the head to the start point of F1 is shown with ‘a’ and the rotary cutter movement in X and Y direction is shown by (L') and (W'), respectively. In this case, after starting the cutting process from F3 and passing through F2, it will reach F1 and complete the abdominal incision and suction processes. This will satisfy the perpendicular movement of the rotary blade that will enter inside the fish body.

The extracted cutting position will be applied in the trout processing

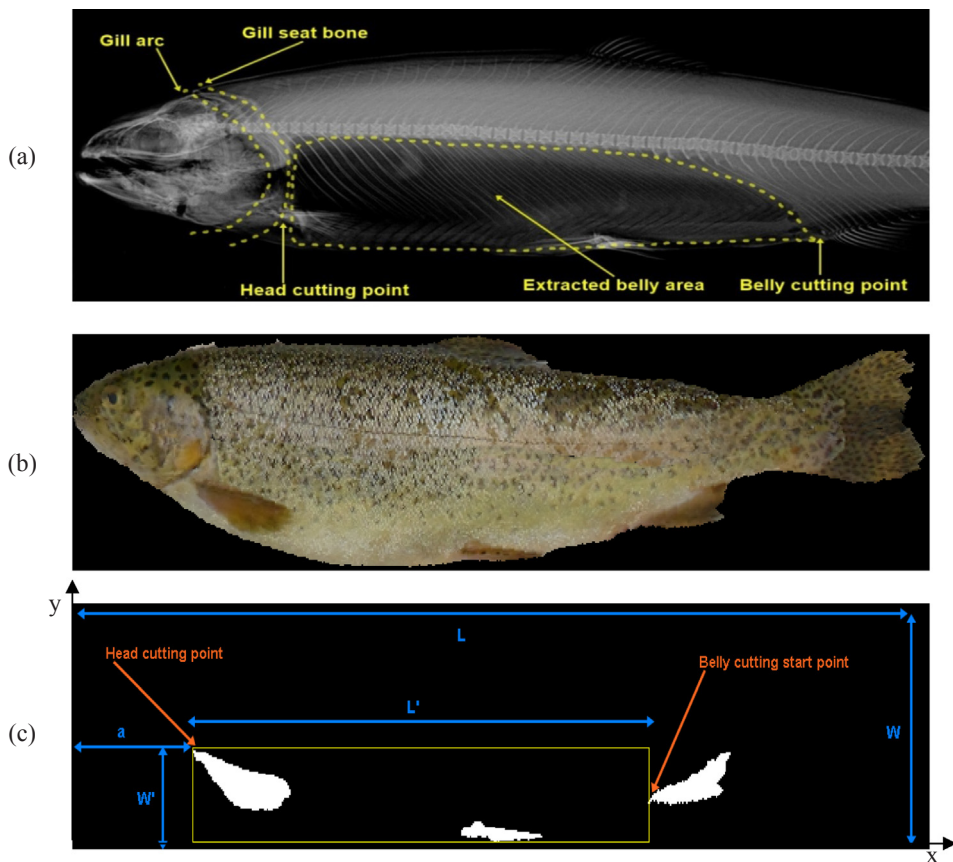


Fig. 16. (a) Processed area of the belly in X-ray image with yellow dash lines and related cutting points for beheading and gutting, (b) sample fish, and (c) exact cutting position of head and belly after processing the images.

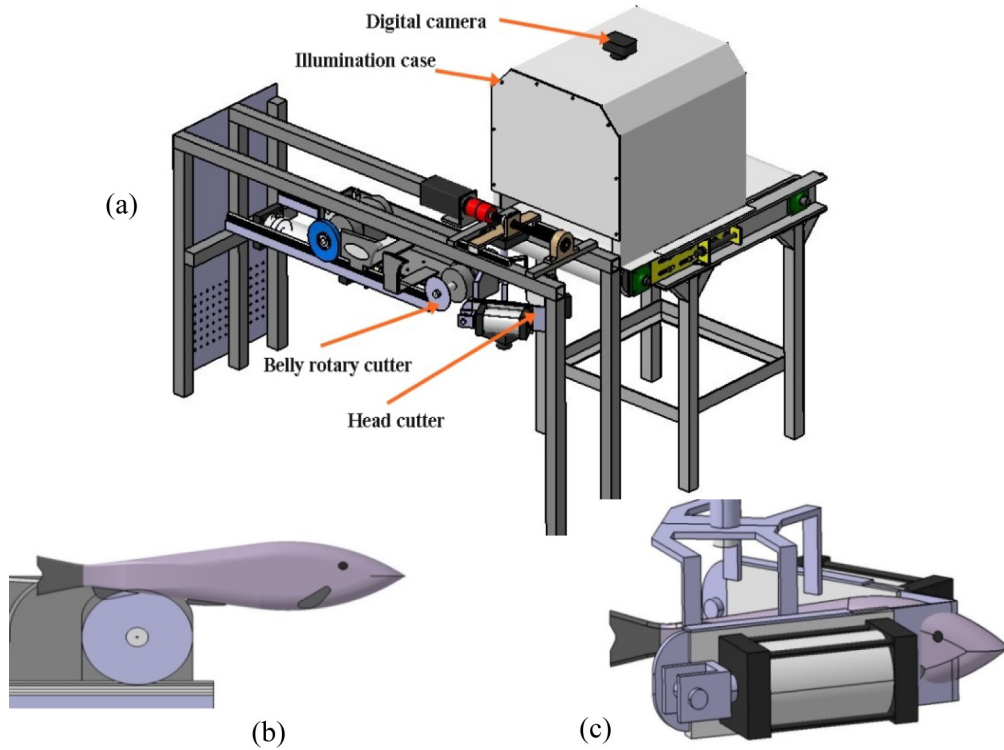


Fig. 17. Mechanical design of the trout beheading and gutting system: (a) complete processing system, (b) gutting subsystem, and (c) beheading subsystem.

system. The complete design of this system is presented in Fig. 17.

The obtained fish size characteristics are used to control the mechanical actuators of the fish processing system. The trout processing machine is designed in Catia R20 software (Fig. 17a) at the University of Tehran and currently is under final construction. The detailed belly and head cutter subsystems are presented in Fig. 17b and c. The mechanical parts of the system are designed to cut the head in 'V' shape. The belly will be longitudinally cut using a rotary knife from anal fin toward the head. The extracted position will be applied to satisfy the most proper cutting and cleaning processes in the intelligent trout processing system with the ability to process different sizes of fish in unsorted samples.

4. Conclusion

In this study, an image processing algorithm was developed to automate a trout processing system. In the first step, by defining an initial centerline and comparing the mean intensity value of each part, the back and belly sides were determined. A secondary line determination procedure facilitated the fin segmentation process. In this case, the belly side was divided into two other parts. Removing the extra parts makes the fin detection process easier since these parts contain the pixels with close intensity values of trout fin. Finally, four fins were detected: pectoral, anal, pelvic, and caudal fins. If fins are precisely segmented, the optimal fish processing will be achieved. Since a threshold was applied in the fin detection step, the area of the fish close to the head was almost without any objects, unless they were smaller than the area of the caudal fin. Therefore, the ratio of the pixels in the head area to the pixels of the tail area resulted in less than '1' in all samples, which was considered the head-tail side detection criterion with entirely successful detection. Among the detected fins, the start point of the pectoral fin was considered for trout beheading. Since the belly intestines exist in the belly cavity in the area between the anal fin and the gills, the skin incision will be made in this distance. To control the perpendicular movement of the belly cutter in different fish samples, the position of the pectoral fin together with the pelvic and anal fins were considered to satisfy the proper belly cutting process. The proposed image processing based pattern resulted in the fin detection algorithm of the trout processing system, which no longer requires any intelligent classification methods like Artificial Neural Networks (ANN) or Support Vector Machines (SVM).

Acknowledgment

The authors would like to acknowledge the financial support of the University of Tehran Science and Technology Park, Iran for this research under grant number "96034".

References

- Atienza-Vanacloig, V., Andreu-García, G., López-García, F., Valiente-González, J.M., Puig-Pons, V., 2016. Vision-based discrimination of tuna individuals in grow-out cages through a fish bending model. *Comput. Electron. Agric.* 130, 142–150.
- Boaman, A.C., Parin, M.A., Zugarramurdi, A., 1997. Efficiency of size sorting of fish. *Int. J. Prod. Econ.* 48 (3), 259–265.
- Buckingham, R., Graham, A., Arnarson, H., Snaeland, P., Davey, P., 2001. Robotics for deheading fish—a case study. *Ind. Robot: Int. J.* 28 (4), 302–309.
- Costa, C., Antonucci, F., Boglione, C., Menesatti, P., Vandepitte, M., Chatain, B., 2013. Automated sorting for size, sex and skeletal anomalies of cultured seabass using external shape analysis. *Aquacult. Eng.* 52, 58–64.
- De, S., Stanley, R.J., Lu, C., Long, R., Antani, S., Thoma, G., Zuna, R., 2013. A fusion-based approach for uterine cervical cancer histology image classification. *Comput. Med. Imaging Graph.* 37 (7), 475–487.
- Dowlati, M., Mohhtasebi, S.S., Omid, M., Razavi, S.H., Jamzad, M., De La Guardia, M., 2013. Freshness assessment of gilthead sea bream (*Sparus aurata*) by machine vision based on gill and eye color changes. *J. Food Eng.* 119 (2), 277–287.
- FAO, 2013. FAOSTAT Database. < http://www.fao.org/fishery/culturedspecies/Oncorhynchus_mykiss > .
- Groschholz, W., & Neumann, R. (2008). U.S. Patent No. 7,427,229. Washington, DC: U.S. Patent and Trademark Office.
- Guttermoen, E., Toldnes, B., Bondø, M., Eilertsen, A., Gravdahl, J.T., Mathiassen, J.R., 2016. A machine vision system for robust sorting of herring fractions. *Food Bioprocess Technol.* 9 (11), 1893–1900.
- Han, Y., Shi, P., 2007. An efficient approach for fish bone detection based on image preprocessing and particle swarm clustering. In: In International Conference on Intelligent Computing. Springer, Berlin, Heidelberg, pp. 940–948.
- Hernández-Ontiveros, J.M., Inzunza-González, E., García-Guerrero, E.E., López-Bonilla, O.R., Infante-Prieto, S.O., Cárdenas-Valdez, J.R., Tlelo-Cuautle, E., 2018. Development and implementation of a fish counter by using an embedded system. *Comput. Electron. Agric.* 145, 53–62.
- Hong, H., Yang, X., You, Z., Cheng, F., 2014. Visual quality detection of aquatic products using machine vision. *Aquacult. Eng.* 63, 62–71.
- Hu, J., Li, D., Duan, Q., Han, Y., Chen, G., Si, X., 2012. Fish species classification by color, texture and multi-class support vector machine using computer vision. *Comput. Electron. Agric.* 88, 133–140.
- Issac, A., Dutta, M.K., Sarkar, B., 2017. Computer vision based method for quality and freshness check for fish from segmented gills. *Comput. Electron. Agric.* 139, 10–21.
- Jain, A., de Silva, C.W., Wu, Q.M.J., 2001. Intelligent fusion of sensor data for product quality assessment in a fish cutting machine. In: In IFSA World Congress and 20th NAFIPS International Conference, 2001. Joint 9th. IEEE, pp. 316–321.
- Ketels, D. (2008). U.S. Patent No. 7,467,995. Washington, DC: U.S. Patent and Trademark Office.
- Khashman, A., 2012. Automatic identification system for raw poultry portions. *J. Food Process Eng* 35 (5), 727–734.
- Krutz, G.W., Gibson, H.G., Cassens, D.L., Zhang, M., 2000. Color vision in forest and wood engineering. *Landscape* 55, 2–9.
- Lee, W.H., Kim, M.S., Lee, H., Delwiche, S.R., Bae, H., Kim, D.Y., Cho, B.K., 2014. Hyperspectral near-infrared imaging for the detection of physical damages of pear. *J. Food Eng.* 130, 1–7.
- Lin, K.C., 2005. On improvement of the computation speed of Otsu's image thresholding. *J. Electron. Imag.* 14 (2), 023011.
- Mendoza, F., Dejmek, P., Aguilera, J.M., 2006. Calibrated color measurements of agricultural foods using image analysis. *Postharvest Biol. Technol.* 41 (3), 285–295.
- Misimi, E., Mathiassen, J.R., Erikson, U., 2007. Computer vision-based sorting of Atlantic salmon (*Salmo salar*) fillets according to their color level. *J. Food Sci.* 72 (1), S030–S35.
- Misimi, E., Erikson, U., Skavhaug, A., 2008. Quality grading of Atlantic salmon (*Salmo salar*) by computer vision. *J. Food Sci.* 73 (5), E211–E217.
- Misimi, E., Øye, E.R., Sture, Ø., Mathiassen, J.R., 2017. Robust classification approach for segmentation of blood defects in cod fillets based on deep convolutional neural networks and support vector machines and calculation of gripper vectors for robotic processing. *Comput. Electron. Agric.* 139, 138–152.
- Mjahad, A., Rosado-Muñoz, A., Bataller-Mompeán, M., Francés-Villora, J.V., Guerrero-Martínez, J.F., 2017. Ventricular Fibrillation and Tachycardia detection from surface ECG using time-frequency representation images as input dataset for machine learning. *Comput. Methods Programs Biomed.* 141, 119–127.
- Muñoz-Benavent, P., Andreu-García, G., Valiente-González, J.M., Atienza-Vanacloig, V., Puig-Pons, V., Espinosa, V., 2018. Enhanced fish bending model for automatic tuna sizing using computer vision. *Comput. Electron. Agric.* 150, 52–61.
- Otsu, N., 1979. A threshold selection method from gray-level histograms. *IEEE Trans. Syst. Man Cybern.* 9, 62–66.
- Paluchowski, L.A., Misimi, E., Grimsmo, L., Randeberg, L.L., 2016. Towards automated sorting of atlantic cod (*Gadus morhua*) roe, milt, and liver—spectral characterization and classification using visible and near-infrared hyperspectral imaging. *Food Contr.* 62, 337–345.
- Paulsohn, C., Dann, A., Rüsch, R., & Brandt, M. (2010). U.S. Patent No. 7,828,635. Washington, DC: U.S. Patent and Trademark Office.
- Poonroy, P., Yodkeaw, P., Sriwai, A., Umongkol, P., Intamoon, S., 2014. Classification of boiled shrimp's shape using image analysis and artificial neural network model. *J. Food Process Eng.* 37 (3), 257–263.
- Ryan, R. M. (2015). U.S. Patent No. 8,986,077. Washington, DC: U.S. Patent and Trademark Office.
- Soille, P., 2013. *Morphological image analysis: principles and applications*. Springer Science & Business Media.
- Storbeck, F., Daan, B., 2001. Fish species recognition using computer vision and a neural network. *Fish. Res.* 51 (1), 11–15.
- Strachan, N.J.C., 1993. Length measurement of fish by computer vision. *Comput. Electron. Agric.* 8 (2), 93–104.
- Teimouri, N., Omid, M., Mollazade, K., Rajabipour, A., 2014. A novel artificial neural networks assisted segmentation algorithm for discriminating almond nut and shell from background and shadow. *Comput. Electron. Agric.* 105, 34–43.
- Teimouri, N., Omid, M., Mollazade, K., Mousazadeh, H., Alimardani, R., Karstoft, H., 2018. On-line separation and sorting of chicken portions using a robust vision-based intelligent modelling approach. *Biosyst. Eng.* 167, 8–20.
- Van Stralen, K.J., Stel, V.S., Reitsma, J.B., Dekker, F.W., Zoccali, C., Jager, K.J., 2009. Diagnostic methods I: sensitivity, specificity, and other measures of accuracy. *Kidney Int.* 75 (12), 1257–1263.
- Wang, K.F., 2014. Quantitative detection of size and centroid of internal defect based on Radon transform and morphological operation in phase-shifting digital speckle pattern interferometry. *NDT E Int.* 63, 50–52.
- White, D.J., Svellingen, C., Strachan, N.J.C., 2006. Automated measurement of species and length of fish by computer vision. *Fish. Res.* 80 (2), 203–210.
- Wu, Q.M., De Silva, C.W., 1993. Automatic adjustment of the cutting position of a vision-based fish processing machine. In: In Communications, Computers and Signal Processing, 1993. IEEE Pacific Rim Conference on IEEE, pp. 702–705.
- Zion, B., Shklyar, A., Karplus, I., 1999. Sorting fish by computer vision. *Comput. Electron. Agric.* 23 (3), 175–187.